# STUDY ON DUST DIFFUSION TRAJECTORY OF UNLOADING POINT IN GANTRY CRANE AREA

by

***Sanxian XIA*[a], *Luqi JIN*[b], *Zuming ZHANG*[b], *Qiao WANG*[c], and *Dasi HE*[b*]**

[a]Technical Management Department, Zhengzhou Rail Transit Co., Ltd., Zhengzhou, China
[b]School of Energy and Environment, Zhong Yuan University of Technology, Zhengzhou, China
[c]School of Energy and Power Engineering, Shandong University, Jinan, China

Original scientific paper
https://doi.org/10.2298/TSCI2503919X

*In order to protect the port environment and effectively reduce the dust concentration at the unloading point the gantry crane area, this paper presents a summary of the dust diffusion rule under different working intensity, falling height, and ore moisture content. The simulation study was conducted to determine the dust diffusion path under different working intensity, falling height, and ore moisture content during ore loading and unloading at the port. The simulation study revealed that during the process of material falling, dust will continuously move in the fluid region. Furthermore, the collision between gravity, particles, and walls will exacerbate the migration range of dust. In the dust diffusion process, the small particle size is concentrated in the upper right corner of the funnel.*

Key words: *dust diffusion, numerical simulation, moisture content*

## Introduction

Since the reform and opening-up, China's economy has experienced a period of rapid development. This has been accompanied by a rapid improvement in the port of ore throughput, which has resulted in a considerable amount of dust being produced during the loading and unloading process. This has led to a number of environmental problems becoming increasingly prominent. The quality of the living environment for residents in the vicinity of the port is not adequately safeguarded. The study of the dust diffusion path during ore handling and the analysis of the influence of environmental factors, including ore falling height and ore quality, on dust diffusion can provide guidance for the control of ore dust diffusion in port.

With regard to the current state of research on dust diffusion models at discharge points, scholars have employed a range of dust diffusion models to numerically simulate the dust diffusion path. Examples of such models include the Euler model [1], the Lagrange model [2], the discrete element method (DEM) coupling model [3], the CFD post model, the discrete phase model (DPM) [4], the volume of fluid (VoF) model [5], and the mixture model [6]. In their study, Patankar and Joseph [1] employed the Euler-Lagrange method to investigate numerically the particle flow. Hu, *et al.* [2] conducted a numerical simulation of coal tunnel blasting by applying the theory of two-phase flow of gases and solids. Gang *et al.* [3] employed the DPM diffusion model and FLUENT software to investigate the impact of dust

* Corresponding author, e-mail: hedasi@zut.edu.cn

removal fan operation on air-flow dynamics within a fully mechanized mining face. Zhang *et al.* [7] employed the DEM coupling model to conduct simulation research on the gas-solid two-phase flow field of grab bucket discharge. The study of dust diffusion paths under different conditions by scholars provides certain reference value for the study of dust diffusion models suitable for loading and unloading points [8]. The numerical scheme based on the mathematical model of multiphase flow of separated particles employs a continuum method for all phases, or alternatively, a continuum method for the fluid phase and a Lagrange method for the particles [9].

In order to effectively reduce the dust concentration during ore loading and unloading in port, a CFD simulation was conducted using the FLUENT software. The simulation involved the analysis of dust diffusion trajectories at the loading and unloading point of gantry crane area under varying water content, falling mass, and wind speed conditions. The resulting dust diffusion range was obtained according to the dust diffusion trajectories under different working conditions.

## Numerical simulation theoretical model

The CFD is a branch of fluid mechanics that employs computer simulation to model actual fluid-flow scenarios. By setting up the simulation conditions and running the simulation, the corresponding results can be obtained. This allows the functionality of the simulation to be evaluated without the need for an experimental set-up [10]. The technology of direct solution of fluid-flow based on the governing equation primarily involves the construction of a geometric model, the division of the grid, the setting of parameters, the setting of boundary conditions, and the solution.

The gas phase follows the Navier-Stokes equation [11]. The continuity equation and the momentum conservation equation are:

$$\frac{\partial}{\partial t}(\varepsilon_{\mathrm{g}}\rho_{\mathrm{g}})+\nabla(\varepsilon_{\mathrm{g}}\rho_{\mathrm{g}}u_{\mathrm{g}})=0 \tag{1}$$

$$\frac{\partial}{\partial t}(\varepsilon_{\mathrm{g}}\rho_{\mathrm{g}}u_{\mathrm{g}})+\nabla(\varepsilon_{\mathrm{g}}\rho_{\mathrm{g}}u_{\mathrm{g}})=-\varepsilon_{\mathrm{g}}\nabla p+\nabla(\varepsilon_{\mathrm{g}}\tau_{\mathrm{g}})+\varepsilon_{\mathrm{g}}\rho_{\mathrm{g}}\mathrm{g}-F_{\text{g-p}} \tag{2}$$

where $\rho_{\mathrm{g}}$ [kgm$^{-3}$] is the density of the air-flow field, $u_{\mathrm{g}}$ [ms$^{-1}$] – the speed of the air-flow field, $p$ [Pa] – the pressure of air-flow field, $\tau_{\mathrm{g}}$ – the viscous stress tensor of the air-flow field, g (= 0.8 m/s$^2$) – the acceleration of gravity, $F_{\text{g-p}}$ – the particle phase and gas force, and $\varepsilon_{\mathrm{g}}$ – the volume fraction of the gas.

In accordance with Newton's second law, the governing equations for the solid phase, which account for collisions between particles and with the wall, are:

$$m_i\frac{\mathrm{d}v_{\mathrm{i}}}{\mathrm{d}t}=m_{\mathrm{i}}\mathrm{g}+f_{\text{p-g,i}}+\sum_{j=1}^{k_i}f_{\text{contact},ij} \tag{3}$$

$$I_{\mathrm{i}}\frac{\mathrm{d}w_{\mathrm{i}}}{\mathrm{d}t}=\sum_{j=1}^{k_i}T_{ij} \tag{4}$$

where $I_{\mathrm{i}}$ [kgm$^2$] is the moment of inertia of particle $i$, $m_{\mathrm{i}}$ [kg] – the mass of particle $i$, $v_{\mathrm{i}}$ [ms$^{-1}$] – the translational velocity of particle $i$, $\omega_{\mathrm{i}}$ [rpm] – the rotation speed of particle $i$, $k_{\mathrm{i}}$ – the number of particles in contact with particle $i$, $T_{ij}$ – the torque, $f_{\text{p-g,I}}$ and $f_{\text{contact},ij}$ [N] – the gas-solid interaction force and contact force with particles and air, respectively.

The mineral powder inherently contains a certain amount of moisture. To facilitate dust suppression, the moisture content of the mineral powder is intentionally increased. Consequently, during the descent of the mineral powder at the unloading point in the gantry crane area, the surface of the powder remains moist. In the process of simulation, the simulated particles must adopt the Hertz-Mindlin with JKR model [12, 13]. During the simulation, it is necessary to employ the Hertz-Mindlin with JKR model for the particles. As the mineral fines descend, adhesive forces emerge between particles and with the wall surfaces. The JKR model relies on the Johnson-Kendall-Roberts theory [14] for determining the normal contact forces between particles or between particles and walls.

$$F_{JKR} = -4\sqrt{\pi\gamma E}\alpha^{\frac{3}{2}} + \frac{4E}{3R}\alpha^3 \tag{5}$$

$$\delta = \frac{\alpha^2}{R} - \sqrt{\frac{4\pi\gamma\alpha}{E}} \tag{6}$$

where $F_{JKR}$ [N] is the normal contact force between particles, $\delta$ [m] – the amount of overlap, $\gamma$ [Nm$^{-1}$] – the surface tension, $E$ [Pa] – the equivalent elastic modulus, $\alpha$ [m] – the amount of tangential overlap, and $R$ [m] – the equivalent contact radius.

## Development and simulation setting of unloading point model in gantry crane area

### *Geometric model and grid division*

In response to the actual conditions of the unloading point in the gantry crane area of Huanghua Port, a site model was reconstructed at a scale of 10:1. Based on this model, the dispersion patterns of dust under various operational conditions were simulated.

The dimensions of the on-site funnel model were increased by a factor of ten. The dimensions of the model are 9.18 m in length, 7.5 m in width, and 9.1 m in height. The specific model is shown in fig. 1.

The parameters set for the 3-D model of the grab bucket is shown in tabs. 1 and 2.

**Table 1. Physical parameters of materials**

| | Poisson's ratio | Shear modulus [Pa] | Density [kgm$^{-3}$] |
|---|---|---|---|
| Simulated particle | 0.4 | 1.1×107 | 1023 |
| Funnel | 0.3 | 7.9×1010 | 7850 |

**Table 2. Material contact coefficient**

| | Recovery coefficient | Coefficient of static friction | Coefficient of rolling friction |
|---|---|---|---|
| Grain-particle | 0.5 | 0.6 | 0.04 |
| Grain - wall surface | 0.5 | 0.4 | 0.05 |

The specific dimensions of the grab bucket are presented in tab. 3. The upper part of fig. 1 represents an enclosed fluid region, while the lower part of the funnel forms a complete fluid region. The study employs a simulation to model the dispersion patterns of dust at emission points within the gantry crane region, while simultaneously considering the impact of environmental factors and the trajectories of ore particles during their descent. The 3-D model of the fluid region is shown in fig. 2.

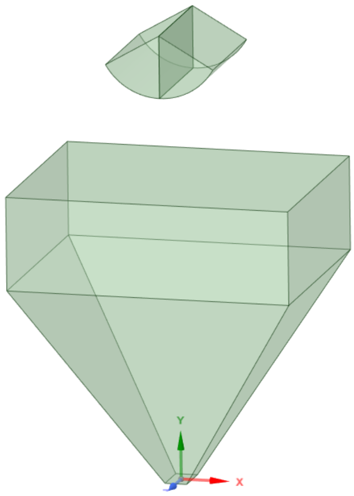

**Figure 1. The 3-D model of grab bucket**

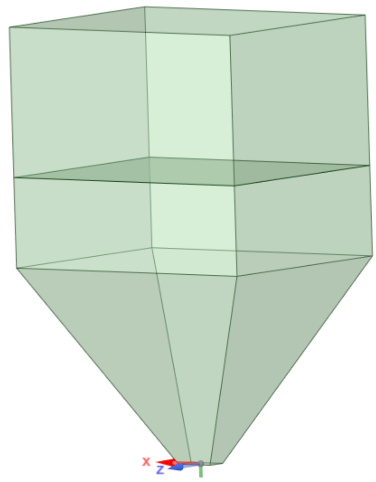

**Figure 2. The 3-D model of fluid region at grab unloading point**

**Table 3. Geometric dimensions of hopper**

| Hopper length and width [m] | Barrel height [m] | Total hopper height [m] | Bottom length and width [m] |
|---|---|---|---|
| 910×750 | 300 | 1120 | 130×70 |

By setting the element size to 10 mm and configuring the mesh generation method for the 3-D model to employ triangles, a mesh with acceptable quality is obtained.

The grid parameters dictate that the grid diagram of the 3-D model of the unloading point in gantry crane area can be divided, as illustrated in fig. 3.

It is evident that the minimum area is greater than 5 m², which meets the condition of solving the calculation. The next step is to name the grid division diagram of the discharge points in the gantry crane area. Subsequently, the fluid domain is delineated by defining the inlet, outlet, and wall boundaries, as illustrated in fig. 4.

The fluid area diagram illustrates the phenomenon of material falling from a height of 0.5 m above the funnel, as well as material falling below this height. During the descent, dust will be generated. The position of the hopper mouth is indicated by the arrow.

### *Boundary conditions*

The model was divided into a grid according to the actual situation on the site and then imported into FLUENT for fluid calculations. In the calculation process, the CFD-DPM model was employed to conduct simulations based on the two-phase flow model and discrete phase model. This involved determining various parameters and boundary conditions for the numerical simulation of the gas phase flow field, as shown in tabs. 4-6.

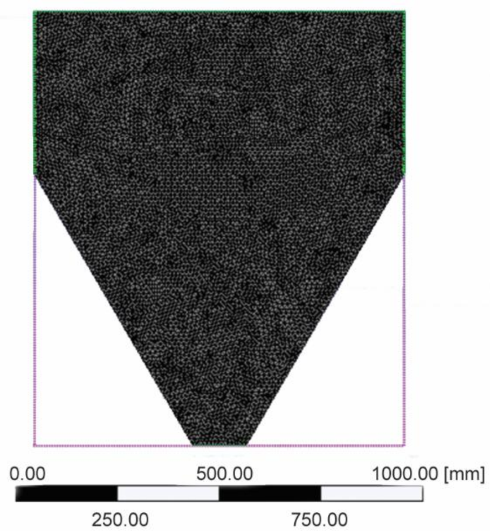


**Figure 3. Grid-division diagram of 3-D model of grab unloading point**

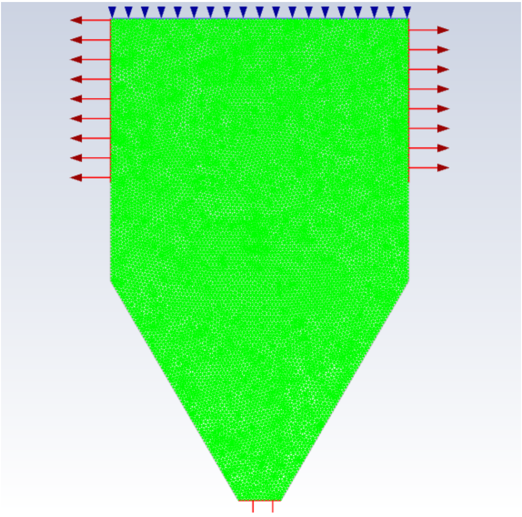

**Figure 4. Fluid region diagram of the 3-D model of grab unloading point**

**Table 4. Parameter setting table of calculation model**

| Model calculation model | Define setting | Model calculation model | Define setting |
|---|---|---|---|
| Time | Transient | Two-phase flow model | Eulerian model |
| Gravity | $Y = -9.81$ m/s$^2$ | Discrete phase model | DPM model |

In order to conduct a simulation, it is necessary to set the relevant parameters of the dust injection source. The following parameters have been set:

**Table 5. Jet source parameter setting table**

| Jet source | Unit | Settings | Remark |
|---|---|---|---|
| Injection source type | | Surface | |
| Jet surface | | Inlet | |
| point | | XYZ | |
| Minimum diameter | [m] | 0.00002 | It depends on the specific mineral species |
| Maximum diameter | [m] | 0.0002 | It depends on the specific mineral species |
| Mean diameter | [m] | 0.00011 | It depends on the specific mineral species |
| Dispersion coefficient | | 10 | |
| Diameter quantity | | 5 | |
| Total flow | [kgs$^{-1}$] | 10 | It depends on the specific mineral species |

**Table 6. Main boundary condition setting table**

| Boundary condition | Unit | Settings |
|---|---|---|
| Entry boundary type | | Velocity inlet |
| Inlet velocity magnitude | [ms$^{-1}$] | 1.5, 3, 4.5, 6 |
| Exit boundary type | | Pressure outlet |
| Wall shear condition | | No slip |

## Simulation of dust diffusion in the process of unloading dust production in gantry crane area

This paper presents a simulation of the dust diffusion trajectory, which is stochastic as shown experimentally in [15], and can be described by a fractal-fractional diffusion model using the two-scale fractal derivatives [16, 17], and can be simulated by the lattice and automata method [18]. In this paper, the orthogonal method [19] was employed to assess the impact of water content, wind speed, and mass-flow rate on the dust production of ore powder during the discharge fall. A simulation of the diffusion trajectory of dust with a material mass of 10 kg/s is presented in fig. 5.

Figure 5 depicts the particle movement track diagram when the particle flow field moves. It can be observed that, during the process of material falling, dust will continue to move within the fluid region. Furthermore, the collision between particles and with walls will exacerbate the migration range of dust. In the context of dust diffusion, the smaller particle size is concentrated in the upper right corner of the funnel. The velocity cloud map is depicted in fig. 6.

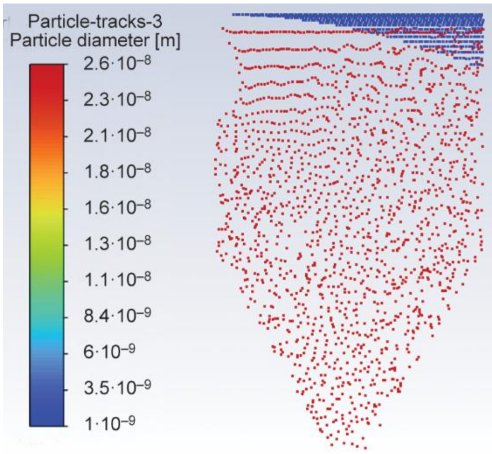


**Figure 5. Trajectory diagram of particle flow field when it moves**

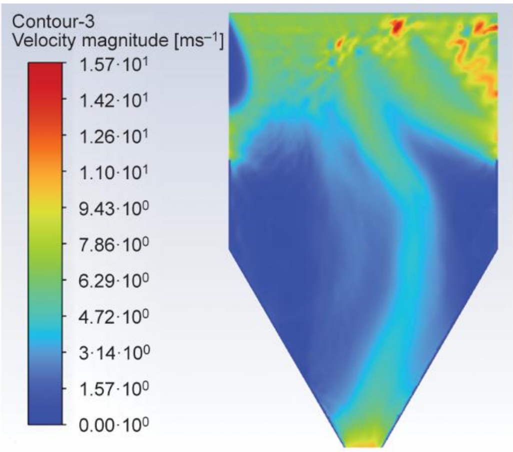


**Figure 6. Velocity cloud map of particle flow field**

During the descent of bauxite, high-velocity particles concentrate at the unloading point in the gantry crane area at the top of the funnel. This concentration is due to the maximum kinetic energy of dust particles at this point, accompanied by the widest dispersion range. This location is the primary target for water-dust suppression strategies.

## Conclusions

To effectively reduce dust concentrations during the ore loading and unloading process at ports, this study employed FLUENT software to simulate the dispersion trajectories of dust at the unloading points of the gantry crane area under varying conditions of moisture content, falling mass, and wind speed. Based on the dispersion trajectories observed under different operational conditions, the derived dust dispersion ranges provide instructive guidance for dust suppression methods during the ore handling process.

Under different operational intensities, the trajectory maps of particle motion in the particle flow field over 1 to 4 seconds reveal that during the descent of the material, dust particles continuously move within the fluid region. The transport range of dust is exacerbated by the interplay of collisions between particles and with the wall surfaces. In the dispersion of dust, smaller particles are concentrated in the upper right of the funnel.

## References

[1] Patankar, N. A., Joseph, D. D., Modeling and Numerical Simulation of Particulate Flows by the Eulerian-Lagrangian approach, *International Journal of Multiphase Flow*, *27* (2001), 10, pp. 1659-1684
[2] Hu, S., *et al.*, Numerical Study of Gas-Solid Two-Phase Flow in a Coal Roadway after Blasting, *Advanced Powder Technology*, *27* (2016), 4, pp. 1607-1617
[3] Gang, Z., *et al.*, Numerical Simulations on Air-flow-Dust Diffusion Rules with the Use of Coal Cutter Dust Removal Fans and Related Engineering Applications in a Fully-Mechanized Coal Mining Face, *Powder Technology*, *339* (2018), Nov., 354-367
[4] Lin, Q., *et al.* Unique Spatial Methane Distribution Caused by Spontaneous Coal Combustion in Coal Mine Goafs: An Experimental Study, *Process Safety and Environmental Protection, Part B*, *116* (2018), May, pp. 199-207
[5] Xiu. Z., *et al.*, Numerical Simulation Study on Dust Pollution Characteristics and Optimal Dust Control Air-flow Rates during Coal Mine Production, *Journal of Cleaner Production*, *248* (2020), 119197
[6] Liu, M., *et al.*, Nonlinear Relationship between Urban Form and Street-Level PM2.5 and CO Based on Mobile Measurements and Gradient Boosting Decision Tree Models, *Building and Environment*, *205* (2021), 108265
[7] Zhang, H., *et al.*, Research on Gas-Solid Two-Phase Flow Field of Grab Discharge Based on CFD-DEM Coupling Simulation (in Chinese), *Mining Research and Development*, *42* (2022), 4, pp. 166-172
[8] Nie, W., *et al.*, Dynamic Dispersion and High-Rise Release of Coal Dust in the Working Surface of a Large-Scale Mine and Application of a New Wet Dust Reduction Technology, *Journal of Cleaner Production*, *351* (2022), 131356
[9] Zwissler, B., *et al.* Thermal Remote Sensing for Moisture Content Monitoring of Mine Tailings: Laboratory Study, *Environmental & Engineering Geoscience*, *23* (2017), 4, pp. 1078-7275
[10] Nylen, J., Sheehan, M., The Impact of Moisture on Lead Concentrate Powder Dust Emissions in Ship-Loading Operations, *Powder Technology*, *394* (2021), Dec., pp. 353-362
[11] Jovanovic, M. M., *et al.*, Thermal Drift in an Inclined Viscous Fluid-flow, *Thermal Science*, *27* (2023), 6A, pp. 4401-4416
[12] Jugder, D., *et al.*, Spatial and Temporal Variations of Dust Concentrations in the Gobi Desert of Mongolia, *Global & Planetary Change*, *78* (2011), 1-2, pp. 14-22
[13] Park, S. U., *et al.*, A Parameterization of Dust Concentration (PM_10) of Dust Events Observed at Erdene in Mongolia Using the Monitored Tower Data, S*cience of the Total Environment*, *409* (2011), 15, pp. 2951-2958
[14] Nietiadi, M. L., *et al.*, An Atomistic Study of Sticking, Bouncing, and Aggregate Destruction in Collisions of Grains with Small Aggregates, *Scientific Reports*, *14* (2024), 1, 7439
[15] He, J.-H., Qian, M. Y., A Fractal Approach to the Diffusion Process of Red Ink in a Saline Water, *Thermal Science*, *26* (2022), 3B, pp. 2447-2451
[16] He, J.-H., El-Dib, Y. O., A Tutorial Introduction to the Two-Scale Fractal Calculus and Its Application to the Fractal Zhiber-Shabat Oscillator, *Fractals*, *29* (2021), 8, 2150268
[17] Li, X. J., *et al.*, A Fractal Two-Phase Flow Model for the Fiber Motion in a Polymer Filling Process, *Fractals*, *28* (2020), 5, 2050093

[18] Filippov, A. E., Popov, V. L., Numerical Simulation of Dynamics of Block Media by Movable Lattice and Movable Automata Methods, *Facta Universitatis series Mechanical Engineering*, *21* (2023), 4, pp. 553-574

[19] Zhang, Y. L., *et al.*, Optimal Design of Impeller for Self-Priming Pump Based on Orthogonal Method, *Scientific Reports*, *13* (2023), 1, 1649

Paper submitted: March 22, 2024
Paper revised: July 1, 2024
Paper accepted: July 7, 2024